



Geochemistry, Geophysics, Geosystems

Supporting Information for

**Production, consumption, and migration of methane
in accetionary prism of southwestern Taiwan**

Nai-Chen Chen¹, Tsanyao Frank Yang¹, Wei-Li Hong^{1,2}, Hsuan-Wen Chen¹, Hsiao-Chi Chen¹, Chin-Yi Hu¹, Yu-Chun Huang¹, Saulwood Lin³, Li-Hung Lin¹, Chih-Chieh Su³, Wei-Zhi Liao³, Chih-Hsien Sun⁴, Pei-Ling Wang³, Tao Yang^{5,6}, Shao-yong Jiang^{5,6}, Char-Shine Liu³, Yunshuen Wang⁷ and San-Hsiung Chung⁷

¹Department of Geosciences, National Taiwan University, Taipei, Taiwan, ²Centre for Arctic Gas Hydrate, Environment and Climate, Department of Geology, UiT The Arctic University of Norway, Tromsø, Norway, ³Institute of Oceanography, National Taiwan University, Taipei, Taiwan, ⁴Exploration and Production Research Institute, CPC Corporation Taiwan, ⁵State Key Laboratory for Mineral Deposits Research, Department of Earth Sciences, Nanjing University, Nanjing 210093, China, ⁶Center of Marine Geochemistry Research, Department of Earth Sciences, Nanjing University, Nanjing, China, ⁷Central Geological Survey, MOEA, Taipei, Taiwan

Contents of this file

Figures S1 to S6

Tables S3 to S5

Additional Supporting Information (Files uploaded separately)

Captions for Tables S1, S2 and S4

Introduction

This supporting information provides details of 1) information of coring sites; 2) raw data; 3) area-based fluxes estimated in the main article; 4) carbon isotope values used in the Fig. 5; 5) evidence supporting for our interpretation; 6) fluxes comparisons and biofiltration efficiency.

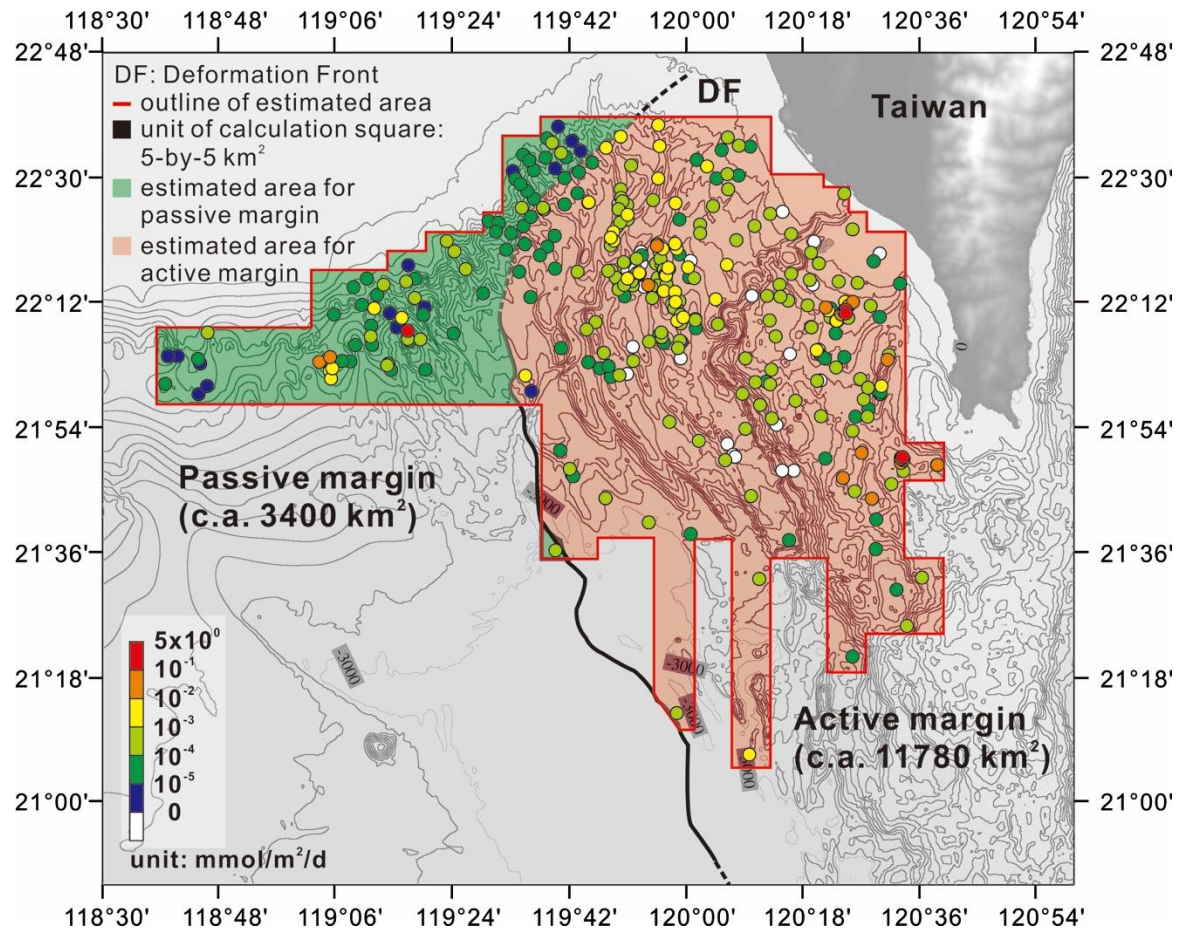


Figure S1. Area coverage for the sampling in active and passive margin used for the area-based rate calculation. The underlay was based on the results of effluxes.

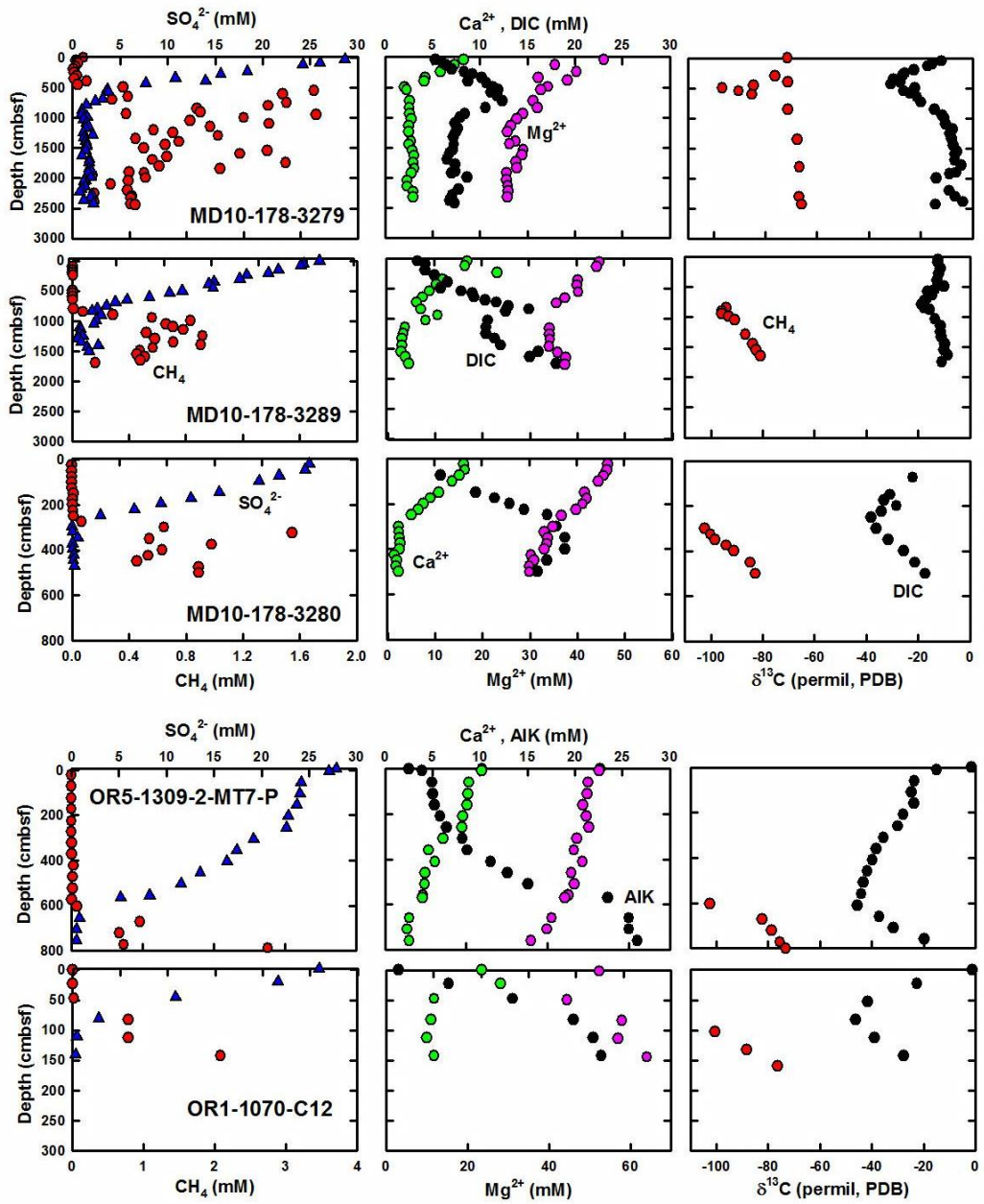


Figure S2. Pore water profiles of data available for carbon mass balance. Data for site 3280 except for Ca^{2+} and Mg^{2+} are adopted from *Lin et al.* [2014].

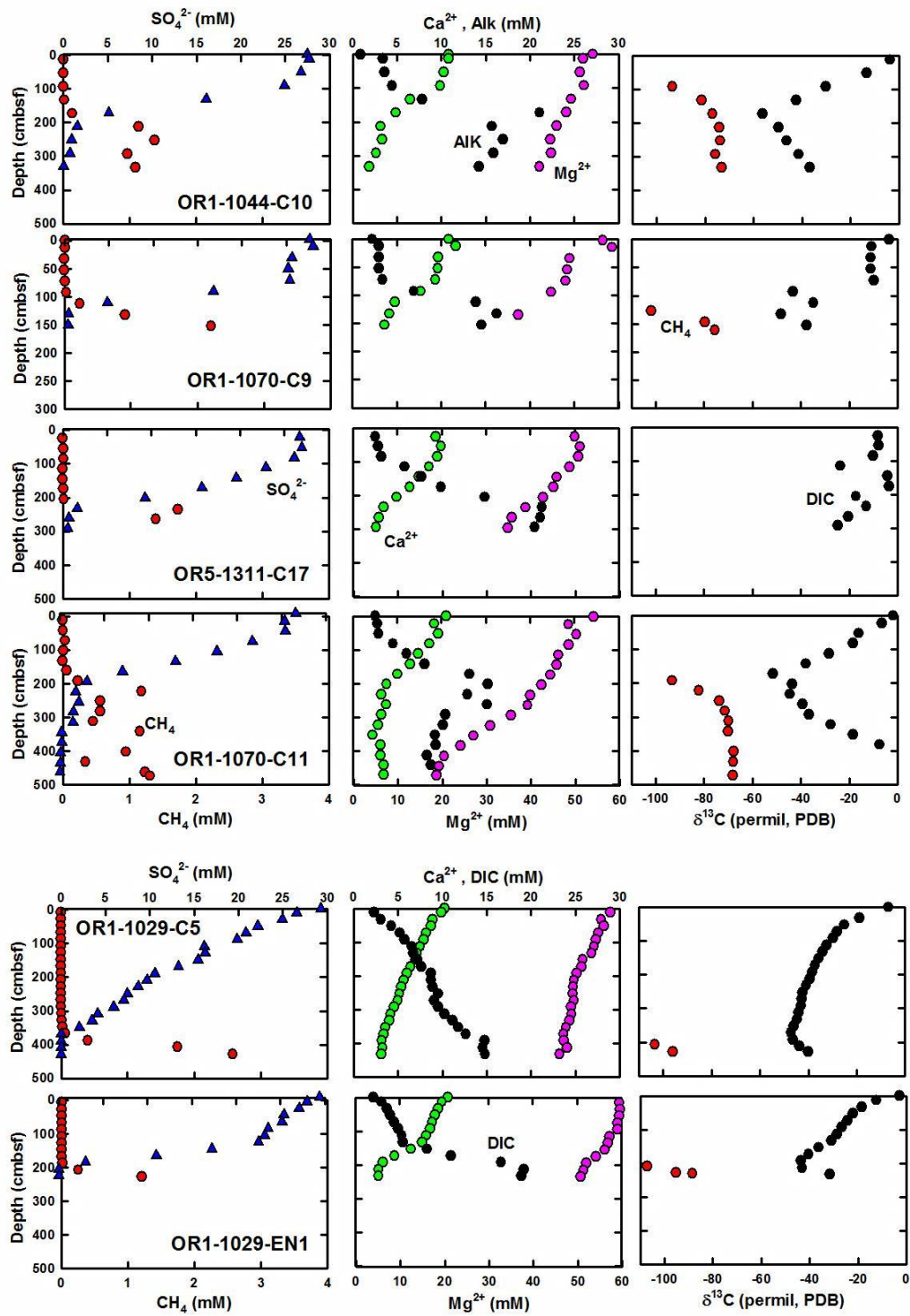


Figure S2. Continued.

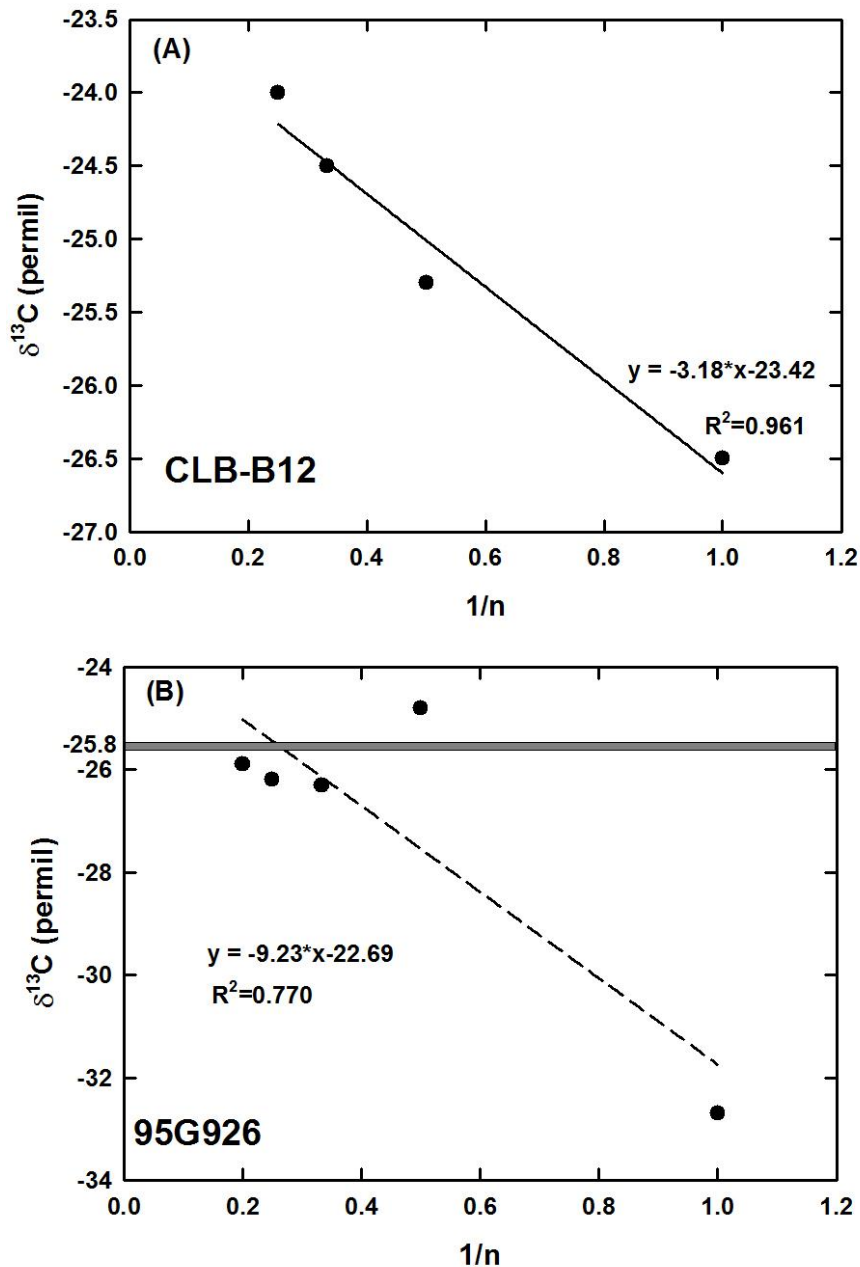


Figure S3. Examples of regression lines used for calculation of deep microbial methane production in different cases. At site CLB-B12 (Table 1), R^2 is more than 0.9 (A). The $\delta^{13}\text{C}$ value of thermogenic methane could be derived from the function of regression line ($x=1$). At site 95G926 (Table 1), R^2 is less than 0.9 (B). Averaged $\delta^{13}\text{C}$ values of C_{2+} (gray bar; the $\delta^{13}\text{C}$ values of C_{2+} generally clustered within $\pm 1\%$) was the $\delta^{13}\text{C}$ value of thermo-hydrocarbon source (-25.8%).

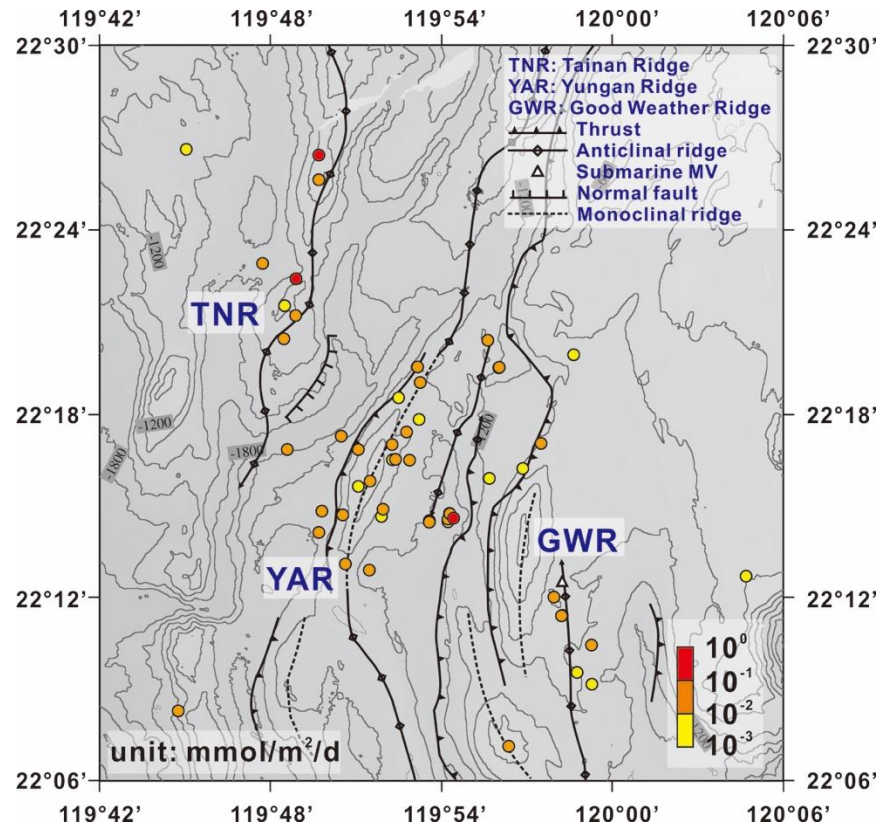


Figure S4. An enlarged view of the red square region in Fig. 2. The tectonic structures are modified from *Lin et al.* [2013].

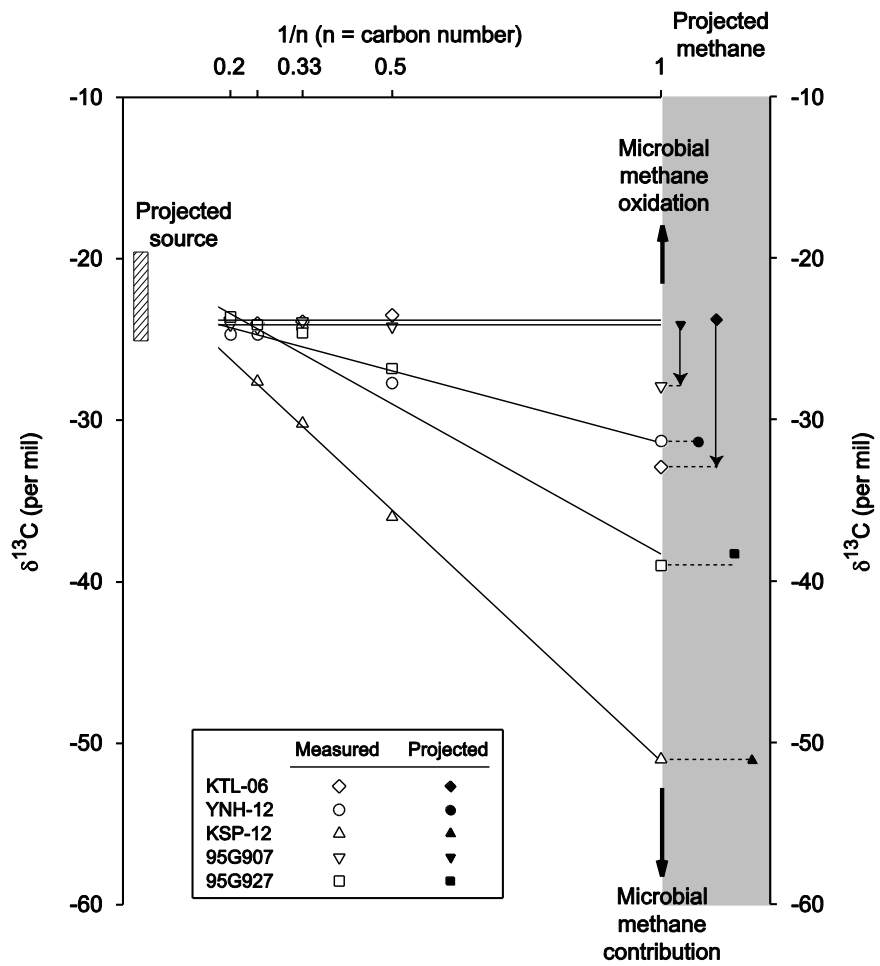


Figure S5. Natural gas plot for five representative gas samples collected from mud volcanoes and seeps onshore southwestern Taiwan (15 sets of data from *Sun et al.* [2008 and 2010] were shown in Table 1). Open symbols represent the measured $\delta^{13}\text{C}$ values of hydrocarbons, whereas solid symbols in the right gray panel indicate the $\delta^{13}\text{C}$ values of pure thermogenic methane projected (shown in solid lines) from the linear regression of all $\delta^{13}\text{C}$ values or averaging $\delta^{13}\text{C}$ values of C_{2+} in the corresponding sample. The measured $\delta^{13}\text{C}$ values of methane are extended by dashed lines to the right panel for comparisons with the projected values (offsets indicated by the thin arrows). The thick arrows at $1/n = 1$ indicates the effects of microbial oxidation and methanogenesis on shifting the $\delta^{13}\text{C}$ values of methane. The hatched area indicates the projected $\delta^{13}\text{C}$ values of hydrocarbon source.

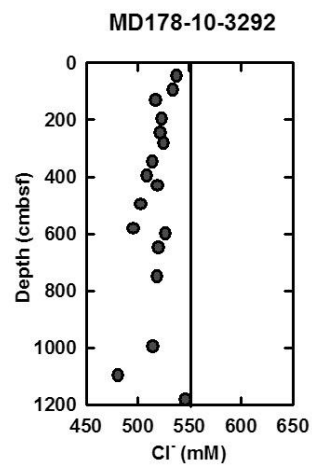


Figure S6. Chloride profile for site MD178-10-3292 showed the possible input of low salinity, deep fluid. This site is located at the anticlinal ridge where a submarine mud volcano is situated (Fig. S4).

Table S1. Details of tectonic features, location of sites and core lengths. Raw data of methane fluxes across SMTZ, effluxes and biofiltration efficiency values.

Table S2. Raw data of methane, sulfate and chloride concentrations.

rates / fluxes	Site										
	C9	C12	MT7	C17	C10	C11	EN1	C5	3289	3279	3280
AOM	22.6	12.6	7.05	4.92	5.43	8.71	24.2	4.32	0.76	12.6	8.55
CR	8.40	4.48	2.78	1.95	1.74	3.13	7.40	0.78	0.20	5.05	2.7
CP	6.71	19.17	2.29	5.34	4.23	5.97	9.64	2.67	1.45	6.07	7.88
ME	2.60	5.74	1.61	2.45	3.53	2.25	0.95	0.36	1.10	0.79	2.51
OSR	5.20	11.5	3.22	4.89	7.06	4.50	1.90	0.72	2.20	1.58	5.02
CH ₄ diffusive flux	5.27	2.23	1.77	8.00	1.70	1.53	24.7	4.53	0.86	3.78	6.02
CH ₄ diffusive flux / AOM	0.23	0.18	0.25	1.62	0.31	0.18	1.02	1.05	1.12	0.30	0.70
AOM/OSR	4.4	1.1	2.2	1.0	0.8	1.9	12.7	6.0	0.3	8.0	1.7
sulfate consumed by AOM (%)	81.3	52.4	68.6	50.2	43.5	66.0	92.7	85.7	25.7	88.8	63.0
Efflux	1.66	0.04		0.10	0.02	0.13	0.03	0.05			
(ME+CR)/AOM	0.5	0.8	0.6	0.9	1.0	0.6	0.3	0.3	1.7	0.5	0.6
Flux from deep source	11.6	2.4	2.7	0.5	0.2	3.3	15.9	3.2		6.7	3.4

Note: Unit: $\times 10^{-2}$ mmol m⁻² d⁻¹

Table S3. Reaction rates within the SMTZ based on the box model and corresponding diffusive fluxes.

Terms	Max	Min	Reference
Sediment mass (R_{acc-M})			
Sediment thickness in trench (H_{tr} ; km)	4.49	1.24	this study; <i>Liao et al. [2016]; Yeh and Hsu [2004]</i>
Length of trench (L_{tr} ; km; 71% of the length of trench considered from 21 to 24.5 °N)	284	284	<i>Chi et al. [2003]; Huang et al. [2006]</i>
Subduction rate (R_{sd} ; km Ma ⁻¹)	76	66	<i>Suppe [1981]; Lundberg et al. [1997]</i>
Bulk sediment density (ρ_{bulk} ; kg km ⁻³)	1.8E12	1.6E12	<i>Wang et al. [2000]</i>
Percentage of matured sediments for methane production (m; with proportion of non-cycling hydrocarbon)			
hydrocarbon potential (PP; g HC / kg rock)	0.5	0.15	<i>Wang et al. [2000]</i>
Total methane generate (Tg Ma ⁻¹)	36,630	1,340	
Percentage of investigated area	60%	60%	
Total methane production (Tg Ma ⁻¹)	21,979	1,406	

Table S4. Parameters used for estimation of thermogenic methane production.

Site	depth (cmbsf)	CH ₄ (mM)	C ₂ H ₆ (μM)	C ₃ H ₈ (μM)	C ₁ /C ₂₊	δ ¹³ C-CH ₄ ‰ (PDB)	δ ² H-CH ₄ ‰ (VSMOW)
Passive margin							
MD10-3264	2046.5	0.61	0.66	b.d.l.	935	-90.5*	
Active margin, lower slope							
OR5-1309-2-MT7-P	800	2.76	b.d.l.	b.d.l.		-73.2	
OR1-1029-C5	428	2.73	1.04	0.03	2551	-95.9	
OR1-1029-EN1	252	9.46	0.35	0.60	9958	-88.4	
OR1-1029-EN2	228	3.54	0.64	0.07	4986	-98.6	
OR1-1044-C10	333	1.09	2.51	b.d.l.	433	-73.2	
OR1-1070-C11	474	1.03	b.d.l.	b.d.l.		-68.1	
OR1-828-GT1	480.5	1.91	0.05	b.d.l.	38115	-83.8	
OR1-860-26	373	1.39	b.d.l.	b.d.l.		-94.2	-178.1
OR1-860-27	226	0.94	b.d.l.	b.d.l.		-72.8	-182.2
OR1-860-28	406	1.66	b.d.l.	b.d.l.		-90.6	-186.9
OR1-978-2N	181.5	1.05	b.d.l.	b.d.l.		-81.4*	
OR1-978-2NL	270.5	0.76	b.d.l.	b.d.l.		-74.0*	
MD178-10-3265	500	0.38	0.18	b.d.l.	2107	-103.0*	
MD178-10-3266	2146.5	0.57	b.d.l.	b.d.l.		-78.1*	
MD178-10-3274	2346.5	0.45	b.d.l.	b.d.l.		-74.4*	
MD178-10-3275	3281.5	0.40	b.d.l.	b.d.l.		-70.2*	
MD178-10-3276	2450.5	1.02	b.d.l.	b.d.l.		-72.7*	
MD178-10-3277	2496.5	1.32	1.61	b.d.l.	819	-68.8*	
MD178-10-3279	2296.5	0.42	3.34	b.d.l.	125	-70.2	-205.0
MD178-10-3280	475	0.89	3.02		294	-85.0*	
MD178-10-3288	2146.5	0.60	b.d.l.			-70.8*	
MD178-10-3292	1096.5	0.36	4.64	b.d.l.	78	-72.1	-225.0
Active margin, upper slope							
OR5-1309-2-MD4-P3	700	1.58	39.76	4.02	36	-38.2	
OR1-1107-96V2	183	1.81	2.4	0.1	730	-37.5	
OR1-1107-MV12-1	102	1.48	7.9	1.4	158	-45.4	
OR1-1107-MV12-3	6	1.26	94.1	38.6	9.2	-35.6	
OR1-1107-MV12-A	112	2.31	5.8	0.8	349	-62.5	
OR1-835-GT39B	463.5	1.32	0.34	b.d.l.	3893	-45.3	-169.9
MD178-10-3289	1650	0.48	5.28	b.d.l.	91	-81.0	-221.3

*Carbon isotopic compositions of methane were measured by a MCIA.

Table S5. Gases concentrations, values of $\delta^{13}\text{C-CH}_4$, and $\delta^2\text{H-CH}_4$ from core bottoms.

Table S6. Rates of AOM and OSR at SMTZ, effluxes and biological filtration efficiency.